BIOMICROFLUIDICS **9**, 014121 (2015)

Distinctive translational and self-rotational motion of lymphoma cells in an optically induced non-rotational alternating current electric field

Wenfeng Liang,[1,2] Ke Zhang,[1] Xieliu Yang,[1] Lianqing Liu,[2,a)] Haibo Yu,[2] and Weijing Zhang[3]
[1]*School of Mechanical Engineering, Shenyang Jianzhu University, Shenyang, China*
[2]*State Key Laboratory of Robotics, Shenyang Institute of Automation, Chinese Academy of Sciences, Shenyang, China*
[3]*Department of Lymphoma, Affiliated Hospital of Military Medical Academy of Sciences, Beijing, China*

(Received 11 January 2015; accepted 10 February 2015; published online 18 February 2015)

In this paper, the translational motion and self-rotational behaviors of the Raji cells, a type of B-cell lymphoma cell, in an optically induced, non-rotational, electric field have been characterized by utilizing a digitally programmable and optically activated microfluidics chip with the assistance of an externally applied AC bias potential. The crossover frequency spectrum of the Raji cells was studied by observing the different linear translation responses of these cells to the positive and negative optically induced dielectrophoresis force generated by a projected light pattern. This digitally projected spot served as the virtual electrode to generate an axisymmetric and non-uniform electric field. Then, the membrane capacitance of the Raji cells could be directly measured. Furthermore, Raji cells under this condition also exhibited a self-rotation behavior. The repeatable and controlled self-rotation speeds of the Raji cells to the externally applied frequency and voltage were systematically investigated and characterized via computer-vision algorithms. The self-rotational speed of the Raji cells reached a maximum value at 60 kHz and demonstrated a quadratic relationship with respect to the applied voltage. Furthermore, optically projected patterns of four orthogonal electrodes were also employed as the virtual electrodes to manipulate the Raji cells. These results demonstrated that Raji cells located at the center of the four electrode pattern could not be self-rotated. Instead any Raji cells that deviated from this center area would also self-rotate. Most importantly, the Raji cells did not exhibit the self-rotational behavior after translating and rotating with respect to the center of any two adjacent electrodes. The spatial distributions of the electric field generated by the optically projected spot and the pattern of four electrodes were also modeled using a finite element numerical simulation. These simulations validated that the electric field distributions were non-uniform and non-rotational. Hence, the non-uniform electric field must play a key role in the self-rotation of the Raji cells. As a whole, this study elucidates an optoelectric-coupled microfluidics-based mechanism for cellular translation and self-rotation that can be used to extract the dielectric properties of the cells without using conventional metal-based microelectrodes. This technique may provide a simpler method for label-free identification of cancerous cells with many associated clinical applications.
[http://dx.doi.org/10.1063/1.4913365]

[a)]Author to whom correspondence should be addressed. Electronic mail: lqliu@sia.cn

I. INTRODUCTION

Research into cell behaviors, such as directed mitosis,[1] separation,[2] differential growth,[3] migration,[4] and apoptosis,[5] is significantly relevant in the life sciences and biomedical fields in order to improve our understanding of cell replication and physiology, tissue culturing, and the diagnosis and treatment of diseases. Substantial efforts have been dedicated to the study of cell behaviors by means of various approaches, such via mechanical,[6] microfluidics,[7] optical,[8] thermal,[9] and electrical[10] mechanisms. A promising category of mechanisms is AC electrokinetics-based techniques. This refers to the use of an externally applied electric field to generate or induce phenomena which include electrophoresis,[11] dielectrophoresis (DEP),[12] AC electro-osmosis (ACEO),[13] induced charge electro-osmosis,[14] AC electro-thermal (ACET),[15] and electro-rotation (ROT).[16] For example, the DEP technique has been demonstrated for separating and purifying cells,[12] characterizing and detecting cell states,[17] determining the dielectric properties of cells,[18] and constructing a 3D tissue culture[19] in an integrated microfluidics-based micro-total-analysis system. Furthermore, this technique has also been explored to promote other bioengineering applications, such as for cell migration[20] and fusion.[21] Additionally, the ROT-based mechanism is another convenient method for extracting the dielectric properties of cells, such as the membrane/cytoplasm/nucleus capacitance and conductance, in a microfluidic chip via a non-uniform electric field. Due to the non-contact and non-destructive advantages for manipulating cells that are suspended in ROT-based chips, a series of studies have focused on the ROT mechanism.[22–25] The effect of ROT on cells can be broadly classified into two categories based on the different electric field conditions: (1) the cells rotating within a rotational AC electric field due to a phase difference in the AC bias potential between the neighboring electrodes; and (2) certain types of cells with specific inherent dielectric properties will also self-rotate in a linearly polarized (i.e., non-rotational) AC electric field. The ROT theory and mechanism in a rotational AC electric field have been clearly defined and understood by researchers; nevertheless, cells rotating in a linearly polarized AC electric field are rarely observed and this phenomenon has been frequently questioned and argued since it was first reported.[26,27] Turcu published a theoretical analysis to explain the reason why certain types of cells will self-rotate in a non-rotational AC electric field along an axis perpendicular to the electric field lines; a possible confirmation that this phenomena may exist under specific conditions.[28] Although the existence of this phenomenon was theoretically predicted by Turcu, actual observations of cells rotating in a linearly polarized AC electric field still remains rare, to the best of our knowledge. Recently, Chuang *et al.*, investigated the uptake of nanoparticles by cells in order to easily obtain their membrane capacitance and conductance. They also observed the rotation of these cells in a linearly polarized AC electric field generated by the metal-based microelectrodes.[29] Moreover, Ouyang *et al.*, described the rotational behavior of pigmented cells with different intrinsic melanin content in a linearly polarized AC electric field. They also experimentally confirmed the rotation phenomenon by seeding foreign particles into cells. Prior to seeding, these cells did not originally self-rotate in the presence of an externally applied non-rotational AC electric field.[30] In the context of these previous results, it is noteworthy to mention that the DEP and ROT techniques refer to the use of metal-based microelectrodes fabricated by conventional photolithographic techniques to generate the spatially non-uniform AC electric field. Consequently, the fixed location of these physical microelectrodes limits the flexibility for dynamic and real-time reconfigurable manipulation, once the electrodes are fabricated. Moreover, the DEP and ROT can only guide cells along a specific trajectory due to the properties of the cells and the fixed configuration of the microelectrodes. This will limit research of the translational and rotational behaviors of cells under an AC electric field.

Instead of using physical microelectrodes to generate the spatially non-uniform electric field, a novel micro-/nano-manipulation technique, called optically induced dielectrophoresis (ODEP) or optoelectronic tweezers (OET)[31] has enabled researchers to dynamically project virtual electrodes that generate the spatially non-uniform and non-rotational AC electric field. These optically projected electrode patterns are digitally generated by commercial animation software and a computer, and subsequently focused by the lenses integrated in a digital

projector. This enables real-time, programmable, and parallel manipulation of cells or particles via ODEP/OET. This technique has already been explored in a large variety of applications, especially in the biomedical and bioengineering fields, such as for discrimination of normal oocytes,[32] manipulation of DNA molecules,[33] mouse embryo selection,[34] and circulating tumor cell isolation.[35] Most importantly, in the bio-related fields, this technique has been demonstrated to work with cells in a non-destructive, non-invasive, and non-contact manner.[35] In the aforementioned applications, the cell behaviors are purely translational motions. Recently, Liang *et al.*, reported that both yeast cells and Ramos (lymphoma) cells underwent the translation and rotation motions simultaneously from the dark areas to the illuminated areas in an OET chip.[36] However, this rotation was performed in a rotational AC electric field. Our team has discovered that only specific types of cells (i.e., Melan-a cells, lymphocytes, and white blood cells) can self-rotate in an OET chip with a non-rotating AC electric field due to the physical properties of cells, such as the uneven distribution of mass within the rotating cells. Furthermore, some type of cells (i.e., RAW 267.4 macrophage cells) did not self-rotate regardless of the applied AC frequency and bias potential.[37] However, in our former study,[37] the explanation on the self-rotation of cells in an ODEP force field was qualitative and only with the investigation of the experimental parameters that affected the self-rotational speed of cells; we did not reveal the reason of the self-rotational phenomenon of cells in an non-rotational electric field. As previously noted,[38] in addition to the DEP force, there simultaneously exist two other types of AC-related electrokinetic forces, namely, ACEO and ACET flows, arising from the interaction of the electric double layers with the tangential component of the electric field and the presence of the non-uniform field resulting in Joule heating, respectively. Consequently, we herein define and use the more general term for an optically induced electrokinetics (OEK) chip.

This paper focuses on the experimental investigation of the transitional and self-rotational behaviors of Raji cells (a type of B-cell lymphoma) in a non-uniform and non-rotational AC electric field in a microfluidics chip. The crossover frequencies of the Raji cells are presented and the corresponding frequency spectrum for measuring the membrane capacitance of the Raji cells is discussed. The self-rotational properties of Raji cells as a function of the applied voltage and frequency are also described. The self-rotational characteristics of the Raji cells are investigated using a pattern of four orthogonal electrodes that are optically projected. The self-rotational behaviors of the Raji cells using the four electrode pattern are broadly categorized. Furthermore, an analysis explaining the self-rotational behavior of the Raji cells in this AC electric field is also elucidated by performing a numerical simulation for two types of optical patterns.

II. MATERIALS AND METHODS

A. OEK chip structure and fabrication procedure

A generalized illustration of the OEK chip used in this study is shown in Fig. 1. The OEK chip consisted of three layers: a top glass substrate was coated with a transparent thin-film of conductive indium tin oxide (ITO) film and used as a top electrode; a microfluidic chamber, that is defined by the gap between the glass layers, is the working area of the chip for suspending the cells to be manipulated (the volume of this chamber is $2\,\text{cm} \times 1\,\text{cm} \times 60\,\mu\text{m}$); a thin film of photoconductive hydrogenated amorphous silicon (a-Si:H) with a thickness of $1\,\mu\text{m}$ that was deposited onto a bottom ITO glass substrate.

The fabrication process for the bottom layer of the OEK chip is described in detail in our previous work.[39] In order to apply an external AC bias potential across the chip, a portion of the a-Si:H layer was etched away to provide an electrical contact to the ITO layer, as shown in Fig. 1. A $5\,\text{mm} \times 8\,\text{mm}$ area of the a-Si:H was patterned through standard photolithography and dry-etched using an Oxford Plasma Lab 80 Plasma Etching System with 2% oxygen and 12.5% CF_4 gas in a 30 mTorr etching chamber, and a 6 min plasma exposure. Then, the chip was rinsed and cleaned with the acetone and DI water before being dried using nitrogen gas. The liquid chamber with a thickness of $\sim 60\,\mu\text{m}$, constructed by using polydimethylsiloxane (PDMS) as a spacer between the glass substrates, formed a microfluidic channel into which the

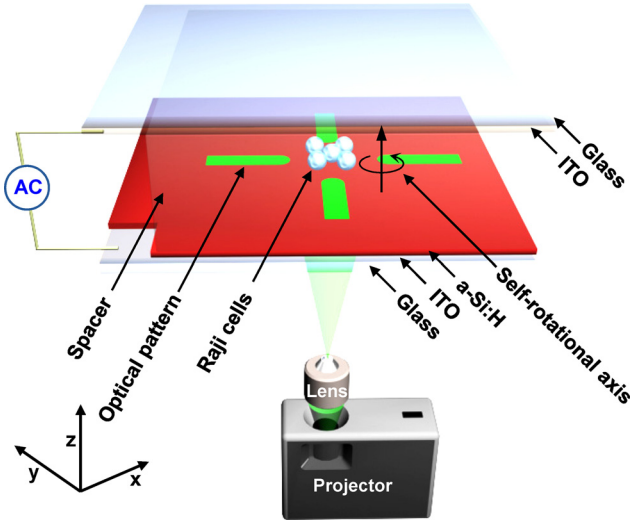

FIG. 1. Three dimensional illustration of the OEK chip. In general, the OEK chip was composed of a top glass substrate coating with a transparent and conductive ITO thin-film, a bottom layer with the a-Si:H deposited onto another ITO glass substrate, and a liquid-filled chamber formed in between was used as the working area. The AC bias potential was applied between the two ITO layers. The schematic of the manipulated Raji cells on the a-Si:H layer indicated that Raji cells could be repelled by the optically projected four electrodes orthogonally aligned to each other.

liquid solutions were injected. In the subsequent fabrication steps, the PDMS layer was permanently bonded to the top glass substrate and to the bottom a-Si:H substrate via an oxygen plasma discharge. In general, this low cost fabrication process for the OEK chip is suitable for mass fabrication.

B. Experimental setup

Fig. 2 is a diagram illustrating the experimental setup for our OEK-based microfluidics platform. Briefly, this platform was composed of an image generation component, an optical transmission element, a cell motion observation section, and a motion control unit. To produce any desired optically projected images, a commercial graphics software package (Flash 11, Adobe, USA) was employed to generate the virtual electrodes in various geometrical configurations. The images were then projected onto the lower surface of the OEK chip via a commercial LCD projector (VPL-F400X, Sony, Japan) connected to a computer. In addition, a condenser lens (MS plan, 50×, Nikon, Japan) fixed between the LCD projector and the OEK chip was used to focus and collimate the optical image onto the OEK chip. The manipulation of the Raji cells was observed and recorded by using a charged coupled device (DH-SV1411FC,

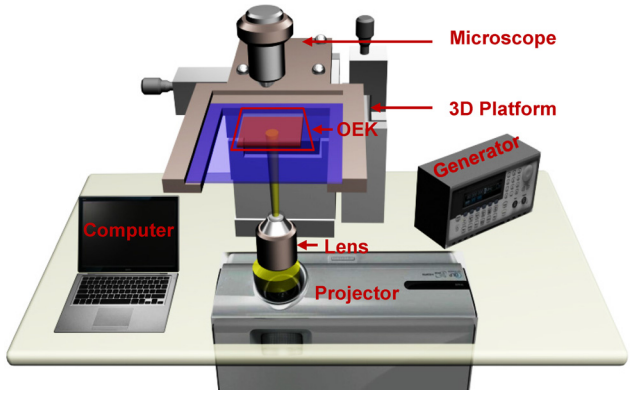

FIG. 2. Illustration of the experimental setup for the OEK platform used for the manipulation of the Raji cells in this study.

DaHeng Image, China) mounted on a microscope (Zoom 160, OPTEM, USA). The OEK chip was set on a three-dimensional digital translation platform (Leetro Automation Co., Ltd, China), which could accurately control the spatial movement of the OEK chip, as well as span the effective working areas on the chip. In order to power the OEK chip to manipulate the Raji cells, an AC bias potential, supplied by a function generator (Agilent 33 522A, USA), was applied to the top and bottom ITO glass substrates, as shown in Fig. 2.

C. Cell preparation, characterization, and counting

A Raji cell line was gifted by Dr. Xiubin Xiao from Affiliated Hospital of Military Medical Academy of Sciences, Beijing, China. The Raji cells were cultured in Roswell Park Memorial Institute (RPMI-1640) culture medium supplemented with 10% (v/v) fetal calf serum, 1% penicillin (v/v) (100 U/ml), and 1% streptomycin (v/v) (100 μg/ml) at 37 °C in an incubator (Model 371, Thermo Scientific, USA) with a humidified atmosphere of 5% CO_2. The sizes of the well cultured Raji cells were measured by an optical microscope (Hirox KH-7700, Japan), and the corresponding size distribution of the Raji cells is shown in Fig. 3. These results showed that the Raji cell diameters under the above same culture conditions were distinctive and ranged from 9 μm to 15 μm. The different diameters for the same group of the Raji cells in the same culture time and culture condition may be due to the fact that Raji cells are during different phases in one cell-cycle. Basically, there exist four phases in a cellular cycle, namely, the G1 gap phase, the synthesis (S) phase, the G2 gap phase, and the mitosis (M) phase, and they are correlated to the size of the cells, the morphology, and changes in organelles such as the DNA contents.[40,41] The mean value of the Raji cell diameter was ~12 μm.

Before each experiment, 1 ml of Raji cell suspension was taken directly out of the culturing flask, and centrifuged at 1000 rpm for 5 min at 4 °C with the supernatant discarded. The collected Raji cells were resuspended into 1 ml of RPMI-1640 culture medium and centrifuged again using the same parameters to remove the residual culture medium. Then, the remaining Raji cells were resuspended into 1 ml of isotonic solution for further experiments. Herein, the isotonic solution used in our experiments consisted of 8.5% (w/v) sucrose, 0.3% (w/v) glucose, and 0.5% (w/v) bovine serum albumin (BSA) in deionized water. The BSA was added to decrease the affinity force between the cells and the a-Si:H substrate of the OEK chip. The conductivity of the isotonic solution was measured to be 1.5×10^{-2} S/m using a conductivity meter (Cond 3110, Germany). After the cellular suspensions were prepared, cells counts were performed using a commercial hemocytometer (Qiujing Co. Ltd., China) to keep the cell concentration of 1×10^5 cells/ml constant for each of the experiments conducted in this study. A 12 μl droplet of cell solution was loaded into the OEK chip, which occupied the entire volume of the OEK chip chamber due to the capillary force. Therefore, there was no net fluid flow in the micro-chamber at initial.

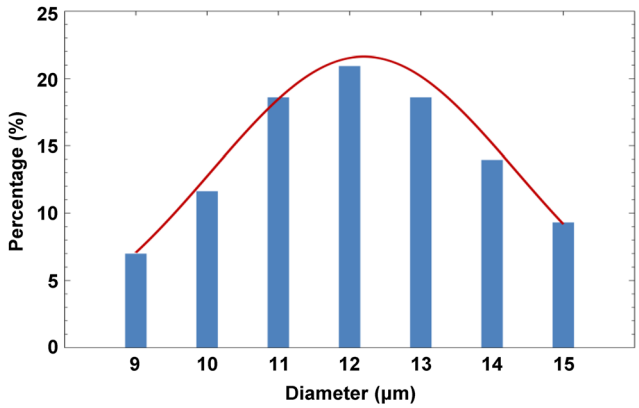

FIG. 3. Distribution of typical sizes of the Raji cells. The measured mean diameter was ~12 μm for the Raji cells.

D. Measurement of the self-rotational velocity of Raji cells

The self-rotational behaviors of Raji cells were recorded by a CCD camera at a fixed frame rate of 15 fps with a resolution of 1392×1040 pixels. The captured image sequences were further processed to obtain the self-rotational speeds by only focusing on the cell, as shown in Fig. 4. The resized cell images were then processed using the computer algorithm for rotation tracking developed by our group.[42,43] This tracking algorithm discriminates the characteristic points for each tracked cell image before recognizing any length changes among of the image sequences in comparison to the first imported image and generates a mapping similarity index. The self-rotational period could be calculated by referring to the similarity index between the image sequences. The equation for the self-rotational speeds of the Raji cells (with units of rpm), as proposed by our group in the previous work, is expressed as[30]

$$n = \frac{5f_{fps}}{\sum_{n=1}^{5} P_n} \times 60, \tag{1}$$

where f_{fps} is the frame rate and P denotes the number of frames required for a single cell to complete one period of the self-rotation. For each cell in this study, 5 consecutive periods were averaged in order to obtain a value for the self-rotational speed.

E. Characterization of the Raji cellular crossover frequency due to the ODEP force

The time-averaged ODEP force (i.e., the DEP force) exerted on cells in a fluidic medium is defined as[44]

$$\langle \vec{F}_{DEP} \rangle = 2\pi R^3 \varepsilon_m \mathrm{Re}[K(\omega)] \nabla |\vec{E}_{rms}|^2, \tag{2}$$

where R is the cell radius, ε_m denotes the permittivity of the surrounding liquid medium, $\vec{E}_{rms}$ is the root-mean-square value of the electric field, ω is the angular frequency, $\omega = 2\pi f$, where f is the applied voltage frequency across the liquid medium, and $\mathrm{Re}(K(\omega))$ is the real part of the Clausius-Mossotti (CM) factor, which reflects the polarization property of the cells against the surrounding liquid medium in a non-uniform electric field.

The DEP force acting on cells can be positive or negative, depending on the sign of the $\mathrm{Re}(K(\omega))$ value under specific applied frequencies of the AC bias potential. Briefly, when the value of the $\mathrm{Re}(K(\omega))$ is greater than zero, the cells will experience a positive DEP force and

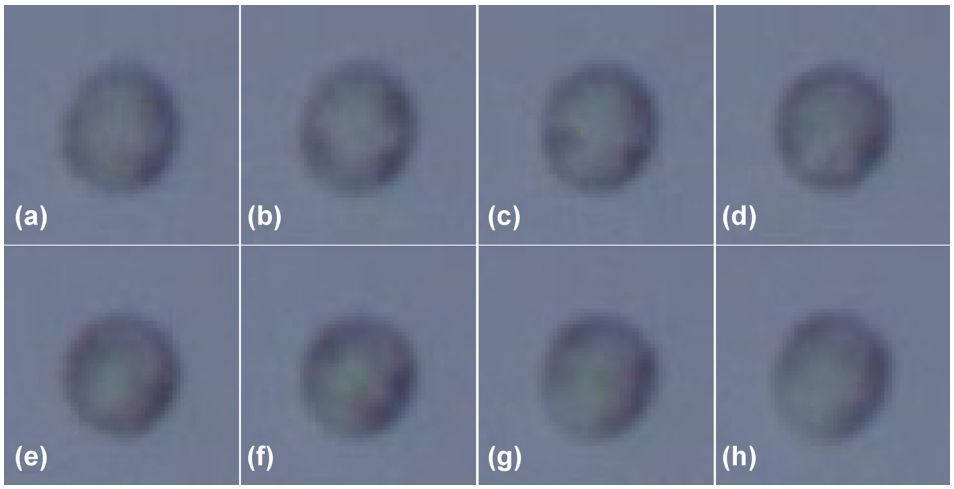

FIG. 4. Time elapsed images of the self-rotation of a Raji cell with a diameter of 14 μm recorded by a CCD camera with a resolution of 1392×1040 pixels. The applied voltage was 10 V_{pp} at a frequency of 40 kHz. A single self-rotational period for the Raji cell under this condition was 15 frames. The corresponding self-rotational speed was 60 rpm.

thus be attracted to the illuminated areas of the OEK chip; conversely, a negative DEP force will be exerted on the cells for a negative value of the $\mathrm{Re}(K(\omega))$ and the cells will be repelled from the illuminated areas of the OEK chip. Our prior work described in Ref. 45 provides a more detailed treatment of how the applied AC waveforms and frequencies can affect the direction and distribution of the DEP force in the OEK chip. A shift of the cells between these two different translation responses (i.e., attracted and repelled motions) with respect to the positive or negative DEP forces occurs where the cellular polarization matches that of the surrounding liquid medium. Then, the corresponding crossover frequency (i.e., the cellular motion would change from an attractive motion to a repulsive motion, or vice versa, at this selected frequency) for this cellular shift is approximately expressed as[46]

$$f_{crossover} = \frac{\sqrt{2}\sigma_m}{2\pi R C_{mem}}, \tag{3}$$

where C_{mem} is the membrane capacitance of the cells and σ_m is the conductivity of the surrounding liquid medium. For Raji cells with different diameters shown in Fig. 3, in this study, we foresee the membrane capacitance would vary, in theory, based on Eq. (3).

III. RESULTS

A. Crossover frequency of the Raji cell by observing translational behaviors

Fig. 5 shows image sequences of the different responses of Raji cells with four different diameters to the positive and negative DEP forces under various applied frequencies with the bias potential at 5 V_{pp}. See online movie for complete experimental details (Multimedia view). As shown in Fig. 5(a), all of the four Raji cells were repelled from the optically projected spot and also observed to undergo a self-rotational behavior simultaneously at frequencies from 20 kHz to 55 kHz in this non-uniform electric field. In general, the Raji cells were found to lyse easily at frequencies lower than 20 kHz. When the frequency was increased to 57 kHz, Raji cell I, with a diameter of 15 μm, was attracted by the optical spot and moved to the edge

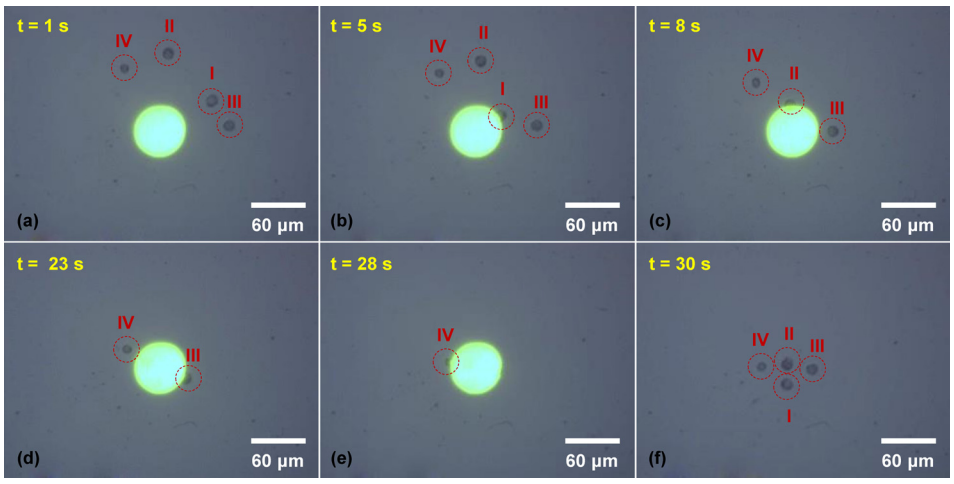

FIG. 5. A series of elapsed time images of the different translation responses of Raji cells to the positive and negative DEP forces under various applied frequencies at an AC bias potential of 5 V_{pp}. The measured diameters for the Raji cells labeled I, II, III, and IV were 15 μm, 14 μm, 13 μm, and 10 μm, respectively. (a) In the frequency range from 20 kHz to 55 kHz, all of the four Raji cells were repelled from the illuminated area and simultaneously underwent a self-rotation. (b) Raji cell I began to move to the edge of the optical spot at a frequency of 57 kHz. (c) When the frequency was increased to 60 kHz, Raji cell II was attracted to the edge of the optical spot and the Raji cell I fully moved to the inner of the optical spot. (d) When the frequency was adjusted to 64 kHz, Raji cell III translated to the edge of the optical spot. (e) Raji cell IV was attracted to the optical spot when the frequency was further increased to 75 kHz. (f) At 30 s, the AC bias potential and the optical spot were turned off, and the final position of the four Raji cells is shown. (Multimedia view) [URL: http://dx.doi.org/10.1063/1.4913365.1]

of the optical spot (Fig. 5(b)). Hence, 57 kHz was determined to be the crossover frequency for Raji cell I. However, Raji cell II, with a diameter of 14 μm, was pulled by the optical spot with a slight translation motion and the other two Raji cells were still located at the initial position with self-rotation behaviors under this condition. Furthermore, when the frequency was gradually changed to 60 kHz, the Raji cell II moved to the edge of the optical spot and the Raji cell I was fully drawn into the inner of the optical spot shown in Fig. 5(c). Thus, 60 kHz was the corresponding crossover frequency for Raji cell II. When the frequency was continuously adjusted to 64 kHz, the Raji cell III with a diameter of 13 μm was pulled into the edge of the optical spot (Fig. 5(d)). The 64 kHz of frequency was the corresponding crossover frequency for the Raji cell III. When the frequency was further increased to 75 kHz, Raji cell IV with a diameter of 10 μm was finally attracted to the edge of the optical spot (Fig. 5(e)). 75 kHz was determined to be the crossover frequency for Raji cell IV. At 30 s, when both the optical spot and the AC bias potential were shut off, the final positions of the four different Raji cells are shown in Fig. 5(f). This means that all four different Raji cells, with different diameters, were manipulated by the positive DEP force once they moved to the optical spot.

To further investigate the trend of the crossover frequencies versus the diameters of the Raji cells, a series of experiments similar to the process described in Fig. 5 were performed systematically. The experimental results shown in Fig. 6 mean that the crossover frequencies for the Raji cells decreased as the cell diameter increased. The corresponding curve also demonstrated that the crossover frequencies for the Raji cells linearly decreased when the cell diameters increased. Furthermore, by using Eq. (3) and combing the experimental results for the crossover frequencies versus the Raji cell diameters, the cell membrane capacitances can easily be extracted, as shown in Fig. 7. The membrane capacitances ranged from 7.90E-3 $\pm$ 0.27E-3 F/m^2 to 9.40E-3 $\pm$ 0.34E-3 F/m^2. The curve fit result for the calculated Raji cell membrane capacitance confirmed the inverse relationship with cell diameter. The decrease in the membrane capacitance as the Raji cell diameters increased may be a result of the Raji cells being in different cell-cycle phases. Furthermore, compared to the Raji cells with smaller diameters, the Raji cells with larger diameters may have a decrease in the effective polarization in this optically induced non-uniform electric field on the OEK chip proposed in this study.

B. Variables affecting the self-rotation speeds of the Raji cells

The impact of the AC frequency and the bias potential on the self-rotational speed of the Raji cells are presented in this section. The same virtual electrode pattern (e.g., a spot with a diameter of 60 μm) is used in these experiments.

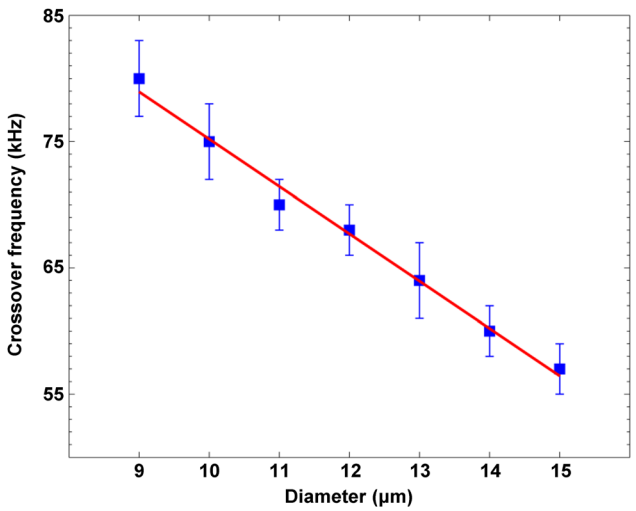

FIG. 6. Crossover frequencies of the Raji cells as a function of the cell diameters. In the figure, each data point is indicated as a mean value $\pm$ standard deviation (n = 5).

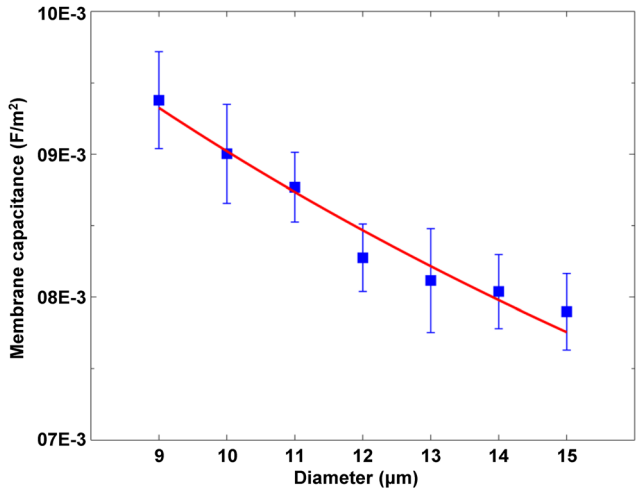

FIG. 7. Capacitances of the Raji cellular membranes with respect to the diameters of the Raji cells. In the figure, each data point is indicated as a mean value ± standard deviation (n = 5).

Fig. 8 shows the self-rotational speeds of Raji cells with respect to the applied AC frequencies at a constant AC bias potential of 10 V_{pp}. The Raji cells, located at a distance of 120 μm from the optical spot center, were recorded and measured to obtain the corresponding self-rotation speeds under different AC frequencies. Due to the large distance between the Raji cell locations and the center of the optical spot, the Raji cells exhibited a much weaker translation motion during the entire experimental process. As plotted in Fig. 8, the Raji cells could self-rotate at the applied frequencies ranging from 20 kHz to 300 kHz using the OEK chip, and the maximum self-rotational speed had a value of 147.0 ± 8.6 rpm at a frequency of 60 kHz. At frequencies less than 20 kHz, the bubbles were easily generated at the illumination area due to the heating effect and the Raji cells were therefore observed to burst. If the frequency was over 300 kHz, the Raji cells did not rotate due to only a smaller voltage drop across the liquid layer of the OEK chip. This experimental result verified that the self-rotational speeds of the Raji cells were linked to the applied frequency. It should be also noted that this ROT spectrum of the self-rotational speeds of the Raji cells versus the applied frequency was very similar to the typical ROT spectrum in a rotational AC electric field.[22–25]

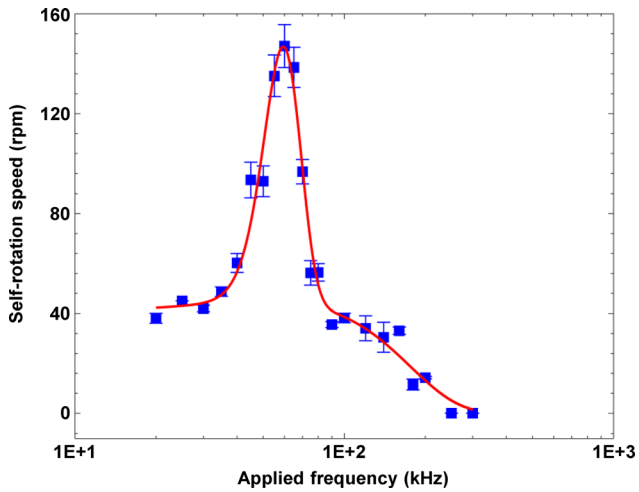

FIG. 8. Self-rotational speeds of the Raji cells versus applied frequencies at a constant AC bias potential of 10 V_{pp}. In the figure, each data point is indicated as a mean value ± standard deviation (n = 5).

Fig. 9 presents the self-rotational speeds of the Raji cells as a function of the applied AC bias potentials from 0 V_{pp} to 10 V_{pp} at a constant frequency of 60 kHz. The tracked Raji cells were originally located at 130 μm from the optical spot center. The Raji cells were at rest from 0 V_{pp} to 1 V_{pp} initially, and then began to rotate at a self-rotational speed of 3.5 ± 0.3 rpm at an AC bias potential of 2 V_{pp}. The self-rotational speeds of the Raji cells increased non-linearly when the applied AC bias potential was linearly increased from 2 V_{pp}, as shown in Fig. 8. The best fit curve shows a quadratic dependence of the self-rotational speeds of the Raji cells on the applied AC bias potential. This relationship was found to be similar to that previously described in typical DEP or ODEP cases,[30,33,37,45] meaning that this self-rotation phenomenon is also related to the electric field.

C. Self-rotation behaviors of Raji cells under four optically projected electrodes

Four optically projected electrodes in an orthogonally aligned pattern, as illustrated in Fig. 1, were employed to manipulate Raji cells and to investigate the parameters associated with their corresponding rotational behaviors. The geometric configuration of the physical four electrode pattern was commonly adopted by traditional ROT experiments to generate a rotational AC electric field, operating on the phase difference in the AC bias potential.[22–25]

Fig. 10 shows the experimental process to observe the Raji cell self-rotation behaviors under the optically projected four electrode pattern. See online movie for complete experimental details (Multimedia view). Raji cell I, with a diameter of 13 μm, was still located at the center area created by the four electrodes when a frequency of 40 kHz at AC bias potential of 5 V_{pp} was applied, as shown in Figs. 10(a) and 10(b), respectively. However, Raji cell I began to deviate from the center area when the frequency was increased to 65 kHz at an AC bias potential of 10 $V_{pp,}$ as shown in Fig. 10(c). Then, Raji cell I would self-rotate at a speed of 20.5 rpm. After 5 s, Raji cell I translated back to the center area again and did not show any further self-rotation when the frequency was increased to 70 kHz, as shown in Fig. 10(d). During the aforementioned process, the Raji cell II and the Raji cell III, both with diameters of 11 μm, were gradually attracted towards the optical pattern and simultaneously exhibited self-rotational behaviors. Raji cell IV, with a diameter of 10 μm, was initially located outside of the field-of-view of the microscope and was also attracted towards the optical pattern. Furthermore, as shown in Fig. 10(e), at a frequency of 75 kHz, the 13 μm Raji cell I deviated again from the center area of the four electrodes due to a positive DEP force; the 10 μm Raji cell IV, that was attracted to the optical pattern with a gradually increasing translation speed from 1.7 μm/s to 12.3 μm/s, also showed self-rotation with a speed of 70.3 rpm; Raji cell V, with a diameter of

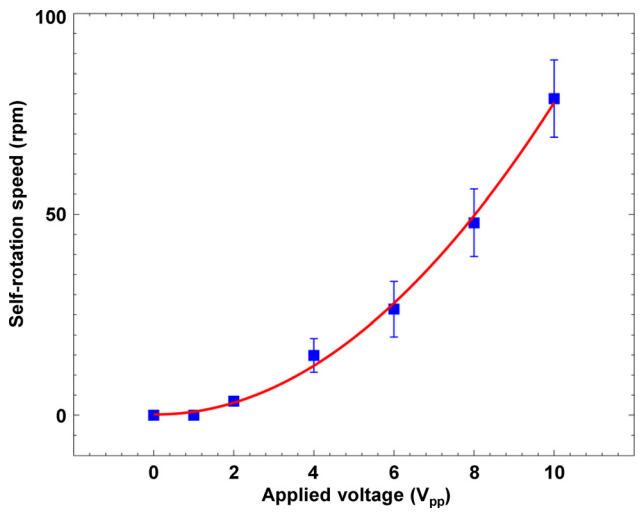

FIG. 9. Self-rotational speeds of the Raji cells versus applied AC bias potentials from 0 V_{pp} to 10 V_{pp} at a constant frequency of 60 kHz. In the figure, each data point is indicated as a mean value ± standard deviation (n = 5).

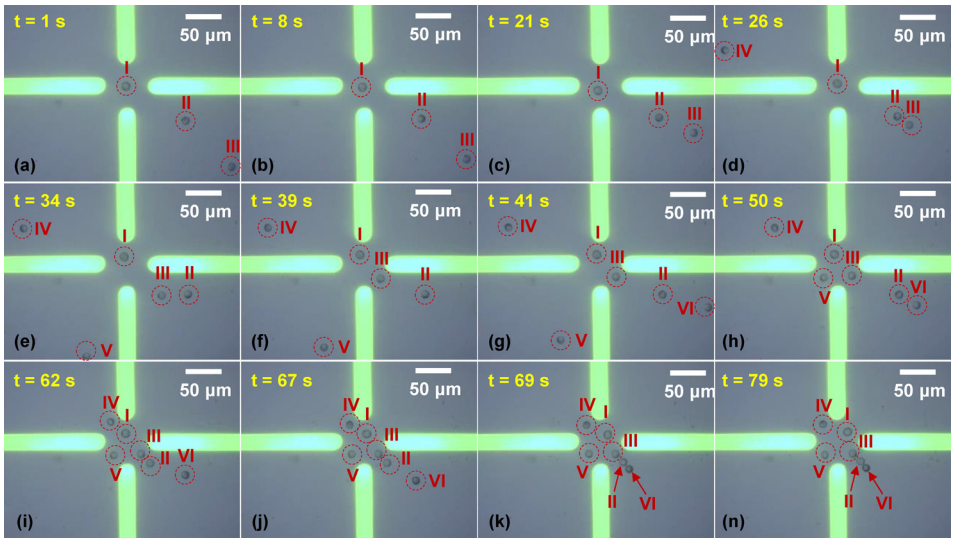

FIG. 10. Experimental results for the self-rotation behaviors of Raji cells under optically projected four orthogonal electrodes at various applied frequencies and AC bias potentials, respectively. The measured diameters for Raji cell I, II, III, IV, V, and VI were 13 μm, 11 μm, 11 μm, 10 μm, 10 μm, and 11 μm, respectively. (a) Raji cells I, II, and III were within the microscope field-of-view in the captured image, and Raji cell I was located at the center of the area created by the four electrodes based patterns; an AC bias potential of 5 V_{pp} at a frequency of 40 kHz was applied. (b) After 8 s, Raji cell I was still located at the center area of the four electrode pattern and did not show any self-rotation motion; Raji cell III was found to undergo a self-rotation motion. (c) When the frequency was adjusted to 65 kHz at an AC bias potential of 10 V_{pp}, Raji cell I began to translate from the center area created by the four electrodes based patterns, Raji cell II began to show the self-rotation behavior, and Raji cell III was attracted to the optical patterns with a self-rotation motion. (d) Once Raji cell I deviated from the central area of the four electrode pattern, Raji cell I could rotate with a self-rotational speed of 20.5 rpm and then translate back to the center area again when the frequency was changed to 70 kHz; both Raji cells II and III moved towards the optical pattern; Raji cell IV was initially located outside of the microscope field-of-view but was gradually attracted towards the center of the electrode pattern. (e) Increasing the frequency to 75 kHz, Raji cell I again deviated from the central area created by the four electrodes, and Raji cells II and III were further attracted to the optical pattern; Raji cell IV was attracted to the optical pattern with a gradually increased translation speed from 1.7 μm/s to 12.3 μm/s and the self-rotational speed of Raji cell IV was 70.3 rpm; Raji cell V was also slowly attracted to the optical pattern; (f) Raji cell III was initially at rest and moving to the central area formed by the two adjacent electrodes. (g) At 41 s, Raji cell VI that was initial outside of the microscope field-of-view was also attracted into the optical pattern when the frequency was increased to 80 kHz; Raji cell V translated towards the optical pattern with an increased speed from 2.2 μm/s to 21.5 μm/s, and simultaneously, Raji cell V also had a self-rotation speed of 102.5 rpm; (h) Raji cell V was also at rest after self-rotating and moving to the central area made by the two adjacent electrodes. (i) Both of the Raji cells II and IV were also at rest after self-rotating and moving to the central areas formed by the two adjacent electrodes, respectively; (j) Raji cell VI moved towards the central area between two adjacent electrodes along the diagonal direction. (k) At 69 s, Raji cell VI was at rest in the central area formed by the two adjacent electrodes and next to Raji cell II; (n) Raji cell I moved to the central area created by the two adjacent electrodes and was finally at rest when the frequency was increased to 100 kHz. (Multimedia view) [URL: http://dx.doi.org/10.1063/1.4913365.2]

10 μm, slowly moved towards the optical pattern. Raji cell III was the first cell to come to rest after self-rotating and translating to the center area between the two adjacent electrodes, as depicted in Fig. 10(f). When the frequency was further adjusted to 80 kHz, as shown in Fig. 10(g), the 10 μm Raji cell V began to accelerate towards the optical pattern at an increased speed from 2.2 μm/s to 21.5 μm/s and a self-rotational speed as high as 102.5 rpm, respectively; Raji cell VI, with a diameter of 11 μm, was slowly attracted towards the optical pattern. At 50 s, Raji cell V came to rest in the center area formed by the two adjacent electrodes. After 12 s, both of the 11 μm Raji cell II and 10 μm Raji cell IV were also at rest after moving to the center area between two adjacent electrodes, respectively. At 69 s, as shown in Fig. 10(k), Raji cell VI was finally at rest and next to Raji cell II. When the frequency was set at 100 kHz, Raji cell I translated to the center area between the two adjacent electrodes and finally stopped. Generally, the self-rotational motion of Raji cells occurred in specific areas of the four electrode pattern. Hence, we consistently identified 2 electrode regions based on the behavior of the cells, i.e., self-rotational and non-rotational areas.

IV. DISCUSSION

A. Numerical simulation of the spatial distributions of the electric field

To ascertain whether the optically induced electric field is rotational or not, a numerical simulation using a commercial finite element method software package (COMSOL Multiphysics 4.3, Sweden) was conducted. Considering the impedance effects of the a-Si:H layer and the AC bias potential across the liquid microchamber, we used the time-harmonic analysis module in the software to model a quasi-static electrical current field with 2D axial symmetry in order to solve Maxwell's equations for the two sub-domains of the a-Si:H layer and the liquid microchamber. The corresponding boundary settings were the same as those discussed in our prior work.[38,45] In this simulation, the liquid conductivity was 1.5×10^{-2} S/m, the dark conductivity of the a-Si:H was 1×10^{-11} S/m, and the photoconductivity was 4×10^{-5} S/m. The experimental values were obtained for our a-Si:H film using a source meter (Keithley 2410, USA). An AC bias potential of 10 V_{pp} with a sine waveform at a frequency of 60 kHz was selected. Moreover, the relative dielectric constant of the liquid and the a-Si:H were 78 and 11, respectively.

The simulation results for the electric field distribution in the liquid microchamber, as induced by the optically projected spot, are shown in Fig. 11. In order to track the change in the electric field over one complete cycle of the AC bias potential, four 90° phase angle increments of the AC voltage waveform were simulated. Generally, we assumed the sinusoidal waveform for the AC bias potential had an initial phase of 10°, herein. Simulation results demonstrated that the electric field was non-uniform; however, over one cycle of the AC bias

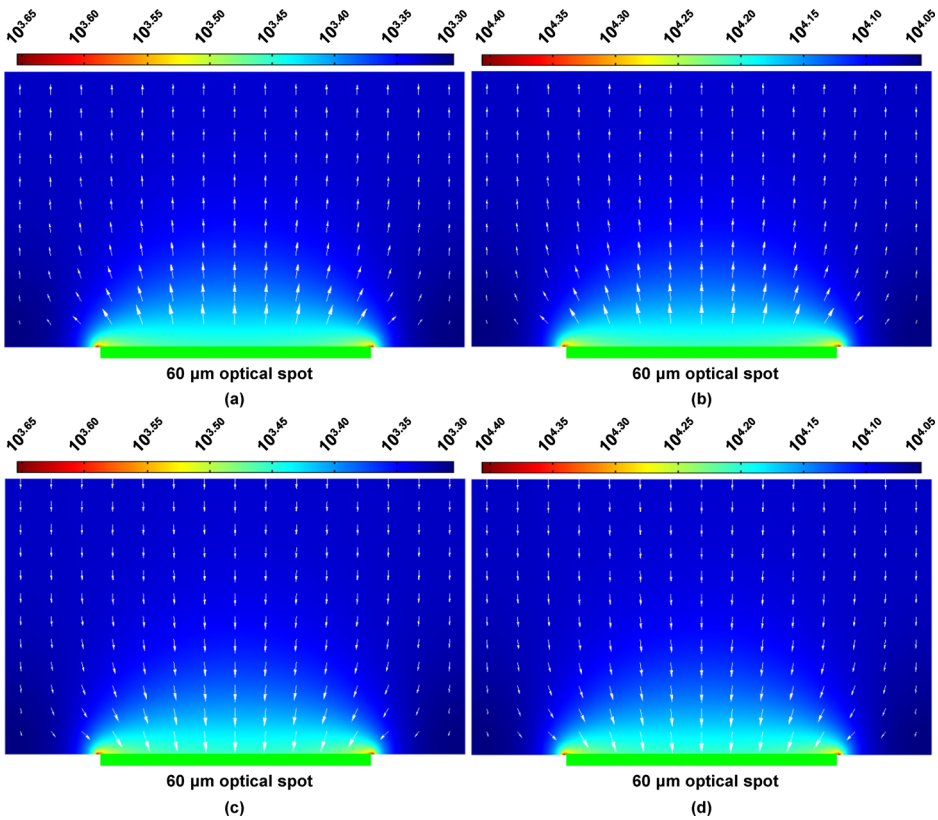

FIG. 11. Simulation results of the electric field distribution induced by the optically projected spot at four different phase angles during one cycle of the AC bias potential. (a) 0°; (b) 90°; (c) 180°; (d) 270°. In all of the four images, the surface colors indicate the magnitude of the electric field and the length of the arrows represented the direction and amplitude of the electric field. To visually enhance the non-uniformity of the electric field in these images, the magnitude of the electric field was plotted on a logarithmic scale.

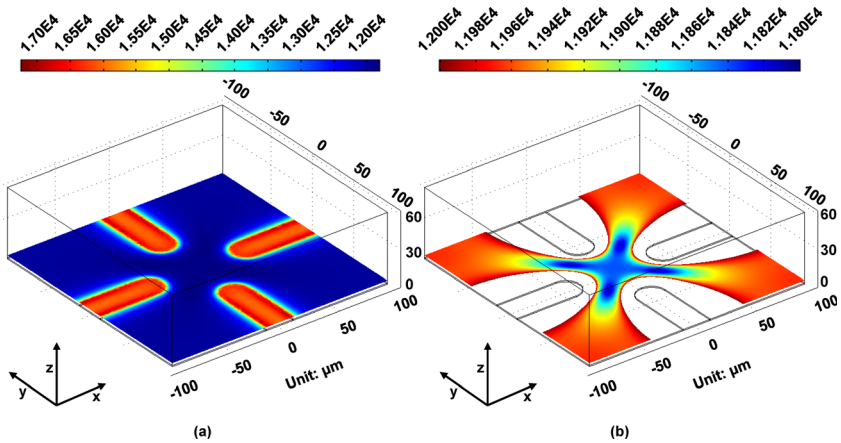

FIG. 12. Simulation results of the electric field distribution generated by the optically projected four electrode pattern. (a) The distribution of the electric field generated by the optical patterns where the maximum electric field in reddish orange is located over the illuminated projected pattern. (b) The electric field distribution at the center areas formed by the four orthogonal electrode patterns which shows the location of the most uniform electric field distribution in blue.

potential, only the direction and magnitude of the electric field changed. Thus, there was indeed no electric field rotational during a cycle of the AC bias potential from the simulation results in Figs. 11(a)–11(d). This implied that the non-uniform electric field played a vital role in the self-rotational behaviors of the Raji cells. As described and discussed in the previous theory about self-rotation by Turcu,[28] an initial electrical torque would be generated when the dipole polarization of specific particles was not parallel to the electric field. Then, this initial torque contributed to growing oscillations resulting in the dynamic rotation.

The spatial electric field distribution induced by the four orthogonal electrode pattern was also calculated using the same simulation method as described in Fig. 11. The time-harmonic analysis 3D module in the software was employed to model a quasi-static electrical current field. These simulation results demonstrated that the magnitude of the electric field was higher around the illuminated areas of the optical patterns (Fig. 12(a)). As shown in Fig. 12(b), the electric field at the center of the four electrode pattern and between any two adjacent electrodes was uniform, i.e., the Raji cells did not show the self-rotation behavior as proven by the experiment results in Fig. 10. Furthermore, the Raji cells exhibited the self-rotational behavior at the non-uniform electric field areas in Fig. 12(b), as verified and described by the experimental results in Fig. 10. This simulation result validates that the non-uniform electric field resulted in the self-rotation behavior in the Raji cells.

B. Self-rotation versus the typical ROT

The self-rotational behavior of cells studied in this paper was significantly different from the typical ROT. This self-rotation did not require the presence of a rotational electric field and the motion could be produced by an axisymmetric and non-uniform electric field, using the same four orthogonal electrode pattern commonly employed in ROT experiments. The single cell could also rotate at locations far from or near to the virtual electrodes. However, there definitely exist some similarity between the self-rotation and the typical ROT effect, since both phenomena were directly related with the electric field distribution and the AC bias potential and frequency. Moreover, the methodology proposed in this paper for extracting the dielectric parameters of the cells also has the advantages of only needing dynamically projected virtual electrodes.

V. CONCLUSION

The translational and self-rotational behaviors of Raji cells have been discussed and described using optically projected patterns to define virtual electrodes on an integrated

microfluidics chip. The distinctive property of the membrane capacitances for Raji cancer cells were derived by determining their ODEP crossover frequencies. By using an optical spot pattern as a virtual electrode, the dependence of the self-rotational speeds of Raji cells on the applied AC frequency and the bias potential were quantified with the aid of computer-vision algorithms. The self-rotational speed of the Raji cells reached a maximum value at a frequency of 60 kHz, with a constant AC bias potential, and also increased with the increase of the AC bias potentials, when the applied frequency was held at constant. Moreover, the self-rotational behaviors of Raji cells in the presence of four optically projected orthogonal electrodes were also experimentally investigated. The areas formed by the four electrode pattern could be broadly classified into regions where the Raji cells could or could not self-rotate. The subsequently numerical simulation of the electric field distribution induced by the projected spot theoretically validated that the induced electric field in the liquid microchamber was non-uniform and non-rotational. Furthermore, electric field distributions for the four electrode pattern were also simulated and these results confirmed that the non-uniform electric field played a pivotal role in the self-rotation behavior of the Raji cell. The methodology proposed in this paper could potentially be developed into a label free, cell-friendly, rapid, low-cost, and automated technique for real-time identification and sorting of cancerous cells by the variations in measured self-rotation speeds and/or the self-rotational and non-self-rotational characteristics for different types of cells. Furthermore, the ability to easily extract the dielectric parameters of the cell membrane by determining the DEP/ODEP crossover frequency could be correlated to the current state of cell growth. This is potentially the most useful application of this method.

ACKNOWLEDGMENTS

This project was funded by the National Natural Science Foundation of China (Project No. 61302003) and the Ministry of Education Innovation Team Plan (Project No. IRT1160).

[1]M. Yeom, J. S. Pendergast, Y. Ohmiya, and S. Yamazaki, Proc. Natl. Acad. Sci. U.S.A. **107**, 9665 (2010).
[2]I. Cima, C. W. Yee, F. S. Iliescu, W. M. Phyo, K. H. Lim, C. Iliescu, and M. H. Tan, Biomicrofluidics **7**, 011810 (2013).
[3]D. Beier, P. Hau, M. Proescholdt, A. Lohmeier, J. Wischhusen, P. J. Oefner, L. Aigner, A. Brawanski, U. Bogdahn, and C. P. Beier, Cancer Res. **67**, 4010 (2007).
[4]M. Junkin and P. K. Wong, Biomaterials **32**, 1848 (2011).
[5]I. Tabas and D. Ron, Nat. Cell Biol. **13**, 184 (2011).
[6]K. Saha, A. J. Keung, E. F. Irwin, Y. Li, L. Little, D. V. Schaffer, and K. E. Healy, Biophys. J. **95**, 4426 (2008).
[7]J. El-Ali, P. K. Sorger, and K. F. Jensen, Nature **442**, 403 (2006).
[8]M. Dao, C. T. Lim, and S. Suresh, J. Mech. Phys. Solids **51**, 2259 (2003).
[9]L. C. Waters, S. C. Jacobson, N. Kroutchinina, J. Khandurina, R. S. Foote, and J. M. Ramsey, Anal. Chem. **70**, 158 (1998).
[10]I. Giaever and C. R. Keese, Proc. Natl. Acad. Sci. U.S.A. **81**, 3761 (1984).
[11]A. J. Dickinson, P. M. Armistead, and N. L. Allbritton, Anal. Chem. **85**, 4797 (2013).
[12]F. Yang, X. Yang, H. Jiang, P. Bulkhaults, P. Wood, W. Hrushesky, and G. Wang, Biomicrofluidics **4**, 013204 (2010).
[13]P. K. Wong, C. Y. Chen, T. H. Wang, and C. M. Ho, Anal. Chem. **76**, 6908 (2004).
[14]T. M. Squires and M. Z. Bazant, J. Fluid Mech. **509**, 217 (2004).
[15]M. Ouyang, R. Mohan, Y. Lu, T. Liu, K. E. Mach, M. L. Y. Sin, M. McComb, J. Joshi, V. Gau, P. K. Wong, and J. C. Liao, Analyst **138**, 3660 (2013).
[16]U. Lei, P. H. Sun, and R. Pethig, Biomicrofluidics **5**, 044109 (2011).
[17]H. Shafiee, M. B. Sano, E. A. Henslee, J. L. Caldwell, and R. V. Davalos, Lab Chip **10**, 438 (2010).
[18]A. C. Sabuncu, J. A. Liu, S. J. Beebe, and A. Beskok, Biomicrofluidics **4**, 021101 (2010).
[19]D. R. Albrecht, G. H. Underhill, T. B. Wassermann, R. L. Sah, and S. N. Bhatia, Nat. Methods **3**, 369 (2006).
[20]D. S. Gray, J. L. Tan, J. Voldman, and C. S. Chen, Biosens. Bioelectron. **19**, 771 (2004).
[21]M. Gel, Y. Kimura, O. Kurosawa, H. Oana, H. Kotera, and M. Washizu, Biomicrofluidics **4**, 022808 (2010).
[22]J. Gimsa, P. Marszalek, U. Loewe, and T. Y. Tsong, Biophys. J. **60**, 749 (1991).
[23]Y. Huang, X. B. Wang, R. Holzel, F. F. Becker, and P. R. C. Gascoyne, Phys. Med. Biol. **40**, 1789 (1995).
[24]R. Hölzel, Biophys. J. **73**, 1103 (1997).
[25]T. Müller, G. Gradl, S. Howitz, S. Shirley, T. Schnelle, and G. Fuhr, Biosens. Bioelectron. **14**, 247 (1999).
[26]H. A. Pohl and J. S. Crane, J. Biophys. **11**, 711 (1971).
[27]M. Mischel and I. Lamprecht, J. Biol. Phys. **11**, 43 (1983).
[28]I. Turcu, J. Phys. A: Math. Gen. **20**, 3301 (1987).
[29]C. H. Chuang, Y. M. Hsu, and C. C. Yeh, Electrophoresis **30**, 1449 (2009).
[30]M. Ouyang, W. K. Cheung, W. Liang, J. D. Mai, W. K. Liu, and W. J. Li, Biomicrofluidics **7**, 054112 (2013).
[31]P. Y. Chiou, A. T. Ohta, and M. C. Wu, Nature **436**, 370 (2005).
[32]H. Hwang, D. H. Lee, W. Choi, and J. K. Park, Biomicrofluidics **3**, 014103 (2009).
[33]Y. H. Lin, C. M. Chang, and G. B. Lee, Opt. Express **17**, 15318 (2009).

[34]J. K. Valley, P. Swinton, W. J. Boscardin, T. F. Lue, P. F. Rinaudo, M. C. Wu, and M. M. Garcia, PLoS One **5**, e10160 (2010).
[35]S. B. Huang, M. H. Wu, Y. H. Lin, C. H. Hsieh, C. L. Yang, H. C. Lin, C. P. Tseng, and G. B. Lee, Lab Chip **13**, 1371 (2013).
[36]Y. L. Liang, Y. P. Huang, Y. S. Lu, M. T. Hou, and J. A. Yeh, Biomicrofluidics **4**, 043003 (2010).
[37]L. H. Chau, W. Liang, F. W. K. Cheung, W. K. Liu, W. J. Li, S. C. Chen, and G. B. Lee, PLoS One **8**, e51577 (2013).
[38]W. Liang, N. Liu, Z. Dong, L. Liu, J. D. Mai, G. B. Lee, and W. J. Li, Sens. Actuators, A **193**, 103 (2013).
[39]S. Wang, W. Liang, Z. Dong, G. B. Lee, and W. J. Li, Micromachines **2**, 431 (2011).
[40]M. Björklund, M. Taipale, M. Varjosalo, J. Saharinen, J. Lahdenperä, and J. Taipale, Nature **439**, 1009 (2006).
[41]G. Ponti, K. Obernier, C. Guinto, L. Jose, L. Bonfanti, and A. Alvarez-Buyll, Proc. Natl. Acad. Sci. U.S.A. **110**, E1045 (2013).
[42]G. Zhang, M. Ouyang, J. Mai, W. J. Li, and W. K. Liu, J. Lab. Autom. **18**, 161 (2013).
[43]Y. Zhao, W. Liang, G. Zhang, J. D. Mai, L. Liu, G. B. Lee, and W. J. Li, Appl. Phys. Lett. **103**, 183702 (2013).
[44]T. B. Jones, *Electromechanics of Particles* (Cambridge University Press, New York, 1995).
[45]W. Liang, S. Wang, Z. Dong, G. B. Lee, and W. J. Li, Micromachines **3**, 492 (2012).
[46]S. Velugotla, S. Pells, H. K. Mjoseng, C. R. E. Duffy, S. Smith, P. D. Sousa, and R. Pethig, Biomicrofluidics **6**, 044113 (2012).